

A Fast Algorithm for the Moments of Bingham Distribution

Yixiang Luo¹, Jie Xu² and Pingwen Zhang³

¹Courant Institute of Mathematical Sciences, New York University, New York 10012, USA

²Department of Mathematics, Purdue University, West Lafayette 47907, USA

³LMAM & School of Mathematical Sciences, Peking University, Beijing 100871, China

Email: yl4507@cims.nyu.edu, xu924@purdue.edu, pzhang@pku.edu.cn

October 15, 2018

Abstract

We propose a fast algorithm for evaluating the moments of Bingham distribution. The calculation is done by piecewise rational approximation, where interpolation and Gaussian integrals are utilized. Numerical test shows that the algorithm reaches the maximal absolute error less than 5×10^{-8} remarkably faster than adaptive numerical quadrature. We apply the algorithm to a model for liquid crystals with the Bingham distribution to examine the defect patterns of rod-like molecules confined in a sphere, and find a different pattern from the Landau-de Gennes theory.

Keywords: Bingham distribution, directional data, piecewise rational approximation, liquid crystals.

1 Introduction

The Bingham distribution is an important antipodally symmetric distribution on the unit sphere \mathbb{S}^2 . Although introduced from a statistical perspective [4], it has found applications in liquid crystals [7, 6, 3, 8], palaeomagnetism [18, 12, 11], and various other fields involving data on the sphere [5, 1, 15, 17, 21].

The density function of the Bingham distribution is given by

$$f(\mathbf{x}|B) = \exp\left(\sum_{i,j=1}^3 B_{ij}x_i x_j\right) / \int_{\mathbb{S}^2} \exp\left(\sum_{i,j=1}^3 B_{ij}x_i x_j\right) d\mathbf{x}, \quad \mathbf{x} \in \mathbb{S}^2, \quad (1)$$

where B is a 3×3 symmetric matrix. A fundamental problem in computation involving the Bingham distribution is evaluating the moments

$$\langle x_1^{n_1} x_2^{n_2} x_3^{n_3} \rangle = \int_{\mathbb{S}^2} f(\mathbf{x}|B) x_1^{n_1} x_2^{n_2} x_3^{n_3} d\mathbf{x}. \quad (2)$$

Denote

$$Z_{n_1 n_2 n_3}(B) = \int_{\mathbb{S}^2} x_1^{n_1} x_2^{n_2} x_3^{n_3} \exp\left(\sum_{i,j=1}^3 B_{ij}x_i x_j\right) d\mathbf{x}. \quad (3)$$

Then the moments can be expressed as $\langle x_1^{n_1} x_2^{n_2} x_3^{n_3} \rangle = Z_{n_1 n_2 n_3}(B)/Z_{000}(B)$.

Even when solving a single problem, the evaluation of moments (2) may need to be done repeatedly. This is a typical case in the simulations of liquid crystals. In each iteration or time step, (2) is computed at each grid point. Generally speaking, the number of space discretization is $O(N^3)$. If we calculate (2) by direct numerical quadrature, it costs $O(N^2)$ operations for every single calculations, leading to a total cost of $O(N^5)$. On the other hand, it should be noted that the density function (1) is determined only by B , not relevant to parameters (and domains, etc.) specified by the problem to be solved. Therefore, it is desirable to have a fast algorithm for the evaluation of (2).

The existing approximations of (2) are designed only for special cases, and are not accurate enough to meet the demand of simulations in many problems. Kent [10] proposed simple expansions for the zeroth and second moments. The relative error is about 0.1%. Kume and Wood [14, 13] developed a method to compute the $Z_{000}(B)$ by using saddle-point approximation. It is accurate for the final estimation result when applying this method in doing maximum likelihood estimation, but not accurate enough for evaluating $Z_{000}(B)$. Moreover, the approximation cannot be easily extended to general $Z_{n_1 n_2 n_3}(B)$. Wang *et. al.* [20] used piecewise linear interpolation to compute B from $Z_{n_1 n_2 n_3}/Z$ where $n_1 + n_2 + n_3 = 2$. This approach works well for B not far from zero matrix, but is inaccurate when it is not the case. We also mention that in [7] the fourth-order moments $Z_{n_1 n_2 n_3}/Z$, ($n_1 + n_2 + n_3 = 4$), are approximated by polynomials of the second-order moments $Z_{n_1 n_2 n_3}$, ($n_1 + n_2 + n_3 = 2$), with a relative error of 5×10^{-4} . This approach is restricted to the cases where B is not involved explicitly.

In this paper, we introduce a fast and accurate algorithm for evaluating $Z_{n_1 n_2 n_3}(B)$. We divide B into three cases and use different approximation method for each case. The main techniques we utilize are interpolation and Gaussian integrals. We have implemented the method for $n_1 + n_2 + n_3 \leq 4$ in a routine named `BinghamMoments`. It is freely available online [16], in which pre-calculations are done and saved as constants in the routine to raise the real-time efficiency. The cost of evaluating $Z_{n_1 n_2 n_3}$ is reduced to $O(1)$ compared with $O(N^2)$ in numerical integration. Numerical experiments show that the absolute error is less than 5×10^{-8} in the routine, while 10^4 times faster than adaptive numerical quadrature with the same accuracy. We apply the method to a liquid crystal model proposed in [3, 8]. The model substitutes the polynomial bulk energy in the widely-used Landau-de Gennes theory with the entropy term expressed by the Bingham distribution. By this substitution the order parameters are confined in the physical range, and it is shown in [8] that this model can be derived from molecular theory. We examine the defect patterns for rod-like molecules confined in a sphere, and find a different structure from the Landau-de Gennes theory. The rest of paper is organized as follows. In Sec. 2, we present the approximation method. The numerical accuracy is examined in Sec. 3. An application to liquid crystals is given in Sec. 4. Concluding remarks are stated in Sec. 5.

2 The approximation method

We diagonalize B using an orthogonal matrix T with $\det T = 1$,

$$B = T \text{diag}(b_1, b_2, b_3) T^T.$$

Then the density function becomes

$$f(\mathbf{x}|B) = \exp\left(\sum_{i=1}^3 b_i(T^T \mathbf{x})_i^2\right) / \int_{\mathbb{S}^2} \exp\left(\sum_{i=1}^3 b_i(T^T \mathbf{x})_i^2\right) d\mathbf{x}. \quad (4)$$

Thus, by the transformation $\mathbf{x} \rightarrow T^T \mathbf{x}$,

$$\begin{aligned} Z_{n_1 n_2 n_3}(B) &= \int_{\mathbb{S}^2} x_1^{n_1} x_2^{n_2} x_3^{n_3} \exp\left(\sum_{i=1}^3 b_i(T^T \mathbf{x})_i^2\right) d\mathbf{x} \\ &= \int_{\mathbb{S}^2} (T\mathbf{x})_1^{n_1} (T\mathbf{x})_2^{n_2} (T\mathbf{x})_3^{n_3} \exp\left(\sum_{i=1}^3 b_i x_i^2\right) d\mathbf{x} \end{aligned} \quad (5)$$

becomes a linear combination of $Z_{m_1 m_2 m_3}(\text{diag}(b_1, b_2, b_3))$. Furthermore, the distribution $f(\mathbf{x}|\text{diag}(b_1, b_2, b_3))$ is invariant under changes $(b_1, b_2, b_3) \rightarrow (b_1 + h, b_2 + h, b_3 + h)$ for any real number h . Without loss of generality, we assume that $b_1 \leq b_2 \leq b_3 = 0$. Denote $Z_{n_1 n_2 n_3}(b_1, b_2) = Z_{n_1 n_2 n_3}(\text{diag}(b_1, b_2, 0))$. It is easy to note that $Z_{n_1 n_2 n_3}(b_1, b_2)$ is nonzero only if n_i are even numbers. Then by $x_3^2 = 1 - x_1^2 - x_2^2$, we can express $Z_{n_1 n_2 n_3}(b_1, b_2)$ linearly by $Z_{nm0}(b_1, b_2)$. Hence it suffices to compute $Z_{nm0}(b_1, b_2)$, denoted in abbreviate by $Z_{nm}(b_1, b_2)$.

Choosing a parameter $d > 0$, we divide $(b_1, b_2) \in (-\infty, 0]^2$ into three regions,

$$(-\infty, -d]^2, \quad (-\infty, -d] \times (-d, 0] \cup (-d, 0] \times (-\infty, -d], \quad (-d, 0]^2.$$

and use different approximation method for each region. The following Gaussian integral is used in the approximation,

$$\int_{\mathbb{R}} x^{2n} \exp(-\alpha x^2) dx = \sqrt{\frac{\pi}{\alpha}} \frac{(2n-1)!!}{(2\alpha)^n}, \quad \alpha > 0. \quad (6)$$

2.1 $b_1, b_2 \leq -d$

We transform the integral domain into the unit circle,

$$\begin{aligned} Z_{nm}(b_1, b_2) &= 2 \iint_{x_1^2 + x_2^2 < 1} x_1^n x_2^m \cdot \exp(b_1 x_1^2 + b_2 x_2^2) \cdot \frac{1}{\sqrt{1 - x_1^2 - x_2^2}} dx_1 dx_2, \\ &= 2 \sum_{j, k \geq 0} \binom{j+k}{j} \frac{(2j+2k-1)!!}{(2j+2k)!!} \iint_{x_1^2 + x_2^2 < 1} x_1^{2j+n} x_2^{2k+m} \exp(b_1 x_1^2 + b_2 x_2^2) dx_1 dx_2. \end{aligned} \quad (7)$$

The series converges because $b_1, b_2 < 0$. We truncate the series at $j+k \leq N_1$. Moreover, if d is large, then $x_1^{2j+n} x_2^{2k+m}$ increases with polynomial rate, while $\exp(b_1 x_1^2 + b_2 x_2^2)$ decreases with exponential rate. Thus we expand the integral domain to \mathbb{R}^2 in the truncated series, which yields the following approximation formula,

$$\begin{aligned} \hat{Z}_{nm}(b_1, b_2) &= 2 \sum_{j+k \leq N_1} \binom{j+k}{j} \frac{(2j+2k-1)!!}{(2j+2k)!!} \iint_{\mathbb{R}^2} x_1^{2j+n} x_2^{2k+m} \exp(b_1 x_1^2 + b_2 x_2^2) dx_1 dx_2. \\ &= \sum_{j+k \leq N_1} \binom{j+k}{j} \frac{(2j+2k-1)!!}{(2j+2k)!!} \sqrt{\frac{\pi^2}{b_1 b_2}} \frac{(2j+n-1)!!(2k+m-1)!!}{(2b_1)^{j+n/2} (2b_2)^{k+m/2}}. \end{aligned} \quad (8)$$

2.2 $b_1 > -d, b_2 \leq -d$ or $b_1 \leq -d, b_2 > -d$

We explain our approximation method by the case $b_1 \leq -d, b_2 > -d$. Rewrite $Z_{nm}(b_1, b_2)$ as

$$Z_{nm}(b_1, b_2) = 4 \int_{-1}^1 x_1^n \cdot \exp(b_1 x_1^2) \cdot g_m(b_2, x_1) dx_1, \quad (9)$$

where

$$g_m(b_2, x_1) = \int_0^{\sqrt{1-x_1^2}} x_2^m \cdot \exp(b_2 x_2^2) \cdot \frac{1}{\sqrt{1-x_1^2-x_2^2}} dx_2. \quad (10)$$

Denote $a = 1 - x_1^2$ and $r = x_2/a$, then we have

$$\begin{aligned} g_m &= \int_0^{\sqrt{a}} x_2^m \cdot \exp(b_2 x_2^2) \cdot \frac{1}{\sqrt{a-x_2^2}} dx_2 \\ &= a^{m/2} \int_0^1 r^m \cdot \exp(b_2 a r^2) \cdot \frac{1}{\sqrt{1-r^2}} dr \\ &= a^{m/2} \cdot \frac{1}{2} \sqrt{\pi} \cdot \frac{\Gamma[(m+1)/2]}{\Gamma[(m+2)/2]} \cdot {}_1F_1\left(\frac{m+1}{2}; \frac{m+2}{2}; b_2 a\right), \end{aligned}$$

where

$$\Gamma(t) = \int_0^\infty x^{t-1} \exp(-x) dx$$

is the gamma function, and ${}_1F_1$ denotes the confluent hypergeometric function.

Note that ${}_1F_1(\frac{m+1}{2}; \frac{m+2}{2}; b_2 a)$ is an entire function about $a \in \mathbb{C}$. Therefore $g_m(b_2, x_1)$ equals to its Taylor's series at $x_1 = 0$ for $x_1 \in (-1, 1)$,

$$g_m(b_2, x_1) = \sum_{j \geq 0} \frac{1}{(2j)!} \left(\frac{\partial^{2j}}{\partial x_1^{2j}} g_m(b_2, 0) \right) x_1^{2j}.$$

Similar to the case $b_1, b_2 \leq -d$, we truncate the series at $j \leq N_2$. Again noticing $b_1 \leq -d$, we expand the integral interval in (9) to \mathbb{R} , leading to the approximation formula

$$\begin{aligned} \hat{Z}_{nm}(b_1, b_2) &= 4 \sum_{j \leq N_2} \frac{1}{(2j)!} \left(\frac{\partial^{2j}}{\partial x_1^{2j}} g_m(b_2, 0) \right) \int_{\mathbb{R}} \exp(b_1 x_1^2) x_1^{2j+n} dx_1 \\ &= 4 \sum_{j \leq N_2} \frac{1}{(2j)!} \left(\frac{\partial^{2j}}{\partial x_1^{2j}} g_m(b_2, 0) \right) \cdot \sqrt{\frac{\pi}{-b_1}} \frac{(2j+n-1)!!}{(-2b_1)^{j+n/2}}. \end{aligned} \quad (11)$$

Next, we explain how to calculate the derivatives $\partial^{2j} g_m(b_2, 0) / \partial x_1^{2j}$. Denote

$$h_1(a) = a^{m/2}, \quad h_2(a) = {}_1F_1\left(\frac{m+1}{2}; \frac{m+2}{2}; b_2 a\right).$$

Then we have

$$\frac{\partial^j g}{\partial a^j} = \frac{1}{2} \sqrt{\pi} \cdot \frac{\Gamma[(m+1)/2]}{\Gamma[(m+2)/2]} \cdot \sum_{k=0}^j \binom{j}{k} \partial_a^k h_1 \cdot \partial_a^{j-k} h_2, \quad (12)$$

with

$$\partial_a^k h_1 = \frac{(m/2)!}{(m/2 - k)!} a^{\frac{m}{2} - k}, \quad k \leq \frac{m}{2}, \quad \partial_a^k h_1 = 0, \quad k > \frac{m}{2}, \quad (13)$$

and

$$\partial_a^k h_2 = b_2^k \left(\frac{m+1}{2} \right)^{(k)} / \left(\frac{m+2}{2} \right)^{(k)} \cdot {}_1F_1 \left(\frac{m+1}{2} + k; \frac{m+2}{2} + k; b_2 a \right) \quad (14)$$

where

$$x^{(0)} = 1, \quad x^{(k)} = x(x+1)(x+2) \cdots (x+k-1)$$

is the rising factorial. Along with

$$\left. \frac{\partial^2 a}{\partial x_1^2} \right|_{x_1=0} = -2, \quad \left. \frac{\partial^i a}{\partial x_1^i} \right|_{x_1=0} = 0, \quad i \neq 2,$$

and the chain rule, we arrive at

$$\left. \frac{\partial^{2j}}{\partial x_1^{2j}} g(x_2^m | b_2, x_1) \right|_{x_1=0} = (-1)^j \cdot \frac{(2j)!}{j!} \cdot \left. \frac{\partial^j g}{\partial a^j} \right|_{a=1}. \quad (15)$$

The derivatives $\partial^{2j} g_m(b_2, 0) / \partial x_1^{2j}$ are functions of b_2 . In the routine `BinghamMoments`, we precompute the values on grid points $b_2 = 0.001k$, and compute the values between the grid points by linear interpolation.

2.3 $b_1 > -d, b_2 > -d$

In this bounded region of (b_1, b_2) , we use interpolation for Z_{00} and Z_{mn}/Z_{00} . We compute them and their derivatives about b_1, b_2 ,

$$\frac{\partial Z_{00}}{\partial b_1} = Z_{20}, \quad \frac{\partial (Z_{nm}/Z_{00})}{\partial b_1} = \frac{Z_{n+2,m} Z_{00} - Z_{nm} Z_{20}}{Z_{00}^2},$$

on the grid $(b_{1,2})_j = -j\Delta b, 0 \leq j \leq -d/\Delta b$. These values are computed in advance and saved as constants in the routine `BinghamMoments`. For Z_{nm} not on the grid points, we calculate with the interpolation described below. Suppose we already know

$$f(x_i, y_j), \quad f_x(x_i, y_j), \quad f_y(x_i, y_j), \quad j = 1, 2.$$

To obtain the approxiamte value $f(x, y)$ on $(x, y) \in [x_1, x_2] \times [y_1, y_2]$, we first calculate

$$f(x, y_1), \quad f(x, y_2), \quad f(x_1, y), \quad f(x_2, y)$$

with third-order Hermite interpolation,

$$\begin{aligned} f(x, y_1) &= f(x_1, y_1) \cdot \left(1 + 2 \frac{x_1 - x}{x_1 - x_2}\right) \left(\frac{x - x_2}{x_1 - x_2}\right)^2 + f(x_2, y_1) \cdot \left(1 + 2 \frac{x_2 - x}{x_2 - x_1}\right) \left(\frac{x - x_1}{x_2 - x_1}\right)^2 \\ &+ f_x(x_1, y_1) \cdot (x - x_1) \left(\frac{x - x_2}{x_1 - x_2}\right)^2 + f_x(x_2, y_1) \cdot (x - x_2) \left(\frac{x - x_1}{x_2 - x_1}\right)^2. \end{aligned}$$

Next we calculate

$$f_y(x, y_1), \quad f_y(x, y_2), \quad f_x(x_1, y), \quad f_x(x_2, y)$$

with linear interpolation,

$$f_y(x, y_1) = f_y(x_1, y_1) \frac{x_2 - x}{x_2 - x_1} + f_y(x_2, y_1) \frac{x - x_1}{x_2 - x_1}.$$

Then we can calculate $f(x, y)$ with third order Hermite interpolation by

$$\begin{aligned} f(x, y) = & f(x_1, y) \cdot \left(1 + 2 \frac{x_1 - x}{x_1 - x_2}\right) \left(\frac{x - x_2}{x_1 - x_2}\right)^2 + f(x_2, y) \cdot \left(1 + 2 \frac{x_2 - x}{x_2 - x_1}\right) \left(\frac{x - x_1}{x_2 - x_1}\right)^2 \\ & + f_x(x_1, y) \cdot (x - x_1) \left(\frac{x - x_2}{x_1 - x_2}\right)^2 + f_x(x_2, y) \cdot (x - x_2) \left(\frac{x - x_1}{x_2 - x_1}\right)^2, \end{aligned} \quad (16)$$

or

$$\begin{aligned} f(x, y) = & f(x, y_1) \cdot \left(1 + 2 \frac{y_1 - y}{y_1 - y_2}\right) \left(\frac{y - y_2}{y_1 - y_2}\right)^2 + f(x, y_2) \cdot \left(1 + 2 \frac{y_2 - y}{y_2 - y_1}\right) \left(\frac{y - y_1}{y_2 - y_1}\right)^2 \\ & + f_y(x, y_1) \cdot (y - y_1) \left(\frac{y - y_2}{y_1 - y_2}\right)^2 + f_y(x, y_2) \cdot (y - y_2) \left(\frac{y - y_1}{y_2 - y_1}\right)^2. \end{aligned} \quad (17)$$

We compute $f(x, y)$ as the average of (16) and (17).

2.4 The value of the parameters

We have introduced four parameters in the above: the size d for dividing the domain, the order of truncation N_1 and N_2 , and the grid size for the interpolation Δb . We choose parameters as $d = 30$, $N_1 = 5$, $N_2 = 5$, $\Delta b = 0.025$ for Z_{00} , and $\Delta b = 0.1$ for Z_{nm}/Z_{00} in the routine `BinghamMoments`, achieving maximal absolute error less than 5×10^{-8} for Z_{00} and $\langle x_1^n x_2^m \rangle$, $n + m \leq 4$. We will verify this in Sec. 3.2. With these parameters, the memory needed for loading precomputed values (including $\partial^{2j} g_m(b_2, 0)/\partial x_1^{2j}$ in the case 2.2, and the values on the grid points in the case 2.3) is about 75MB, which is available for common computers.

3 Numerical accuracy

3.1 Error estimate

We give an error estimate for the case 2.1 with some special functions. Denote

$$F(x) = e^{-x^2} \int_0^x e^{t^2} dt$$

as the Dawson function,

$$\gamma(n, x) = \int_0^x t^{n-1} e^{-t} dt$$

as the lower incomplete gamma function, and

$$\alpha_n(z) = E_{-n}(z) = n! z^{-n-1} e^{-z} \left(1 + z + \frac{z^2}{2!} + \cdots + \frac{z^n}{n!}\right)$$

as the exponential integral function.

Theorem 3.1. Let \hat{Z}_{nm} be defined in (8) and denote $N = N_1$. For $b_1, b_2 \leq -d$, it holds

$$\begin{aligned} |Z_{nm} - \hat{Z}_{nm}| &\leq 4\pi \frac{F(\sqrt{d})}{\sqrt{d}} - 2\pi \sum_{j=0}^N \frac{(2j-1)!!}{(2j)!!} \cdot d^{-j-1} \gamma(j+1, d) \\ &\quad + 2\pi \sum_{j=0}^{N+\max(n,m)} \frac{(2j-1)!!}{(2j)!!} \alpha_j(d). \end{aligned} \quad (18)$$

Proof. We can divide the error into two parts:

$$\begin{aligned} e_1 &= Z_{nm}(b_1, b_2) - 2 \iint_{B(0,1)} x_1^n x_2^m \exp(b_1 x_1^2 + b_2 x_2^2) \sum_{j=0}^N \frac{(2j-1)!!}{(2j)!!} \cdot (x_1^2 + x_2^2)^j \, d\mathbf{x} \\ &= 2 \iint_{B(0,1)} x_1^n x_2^m \exp(b_1 x_1^2 + b_2 x_2^2) \sum_{j>N} \frac{(2j-1)!!}{(2j)!!} (x_1^2 + x_2^2)^j \, d\mathbf{x}, \end{aligned} \quad (19)$$

$$e_2 = 2 \iint_{\mathbb{R}^2 \setminus B(0,1)} x_1^n x_2^m \exp(b_1 x_1^2 + b_2 x_2^2) \sum_{j=0}^N \frac{(2j-1)!!}{(2j)!!} (x_1^2 + x_2^2)^j \, d\mathbf{x}. \quad (20)$$

For e_1 , we have

$$\begin{aligned} e_1 &\leq 2 \iint_{B(0,1)} \exp(-d(x_1^2 + x_2^2)) \sum_{j>N} \frac{(2j-1)!!}{(2j)!!} (x_1^2 + x_2^2)^j \, d\mathbf{x} \\ &= 2 \iint_{B(0,1)} \exp(-d(x_1^2 + x_2^2)) \left[\frac{1}{\sqrt{1-x_1^2-x_2^2}} - \sum_{j \leq N} \frac{(2j-1)!!}{(2j)!!} (x_1^2 + x_2^2)^j \right] \, d\mathbf{x} \\ &\leq 4\pi \int_0^1 e^{-dr^2} \frac{r}{1-r^2} \, dr - 4\pi \sum_{j=0}^N \frac{(2j-1)!!}{(2j)!!} \int_0^1 r^{2j+1} e^{-dr^2} \, dr \\ &= 4\pi \frac{F(\sqrt{d})}{\sqrt{d}} - 2\pi \sum_{j=0}^N \frac{(2j-1)!!}{(2j)!!} d^{-j-1} \gamma(j+1, d). \end{aligned} \quad (21)$$

In the above, we use the polar coordinate transformation $x_1 = r \cos \theta$, $x_2 = r \sin \theta$. For e_2 , denote $M = \max\{n, m\}$, then we have

$$e_2 \leq 4\pi \sum_{j=0}^{N+M} \frac{(2j-1)!!}{(2j)!!} \int_1^\infty r^{2j+1} e^{-dr^2} \, dr = 2\pi \sum_{j=0}^{N+M} \frac{(2j-1)!!}{(2j)!!} \alpha_n(d). \quad (22)$$

Combining (21) and (22), we get (18). \square

For our chosen parameters $d = 30$ and $N_1 = 5$, the upper bound given by (18) is 6.038×10^{-8} for $n + m \leq 4$. We also give the upper bound calculated from (18) for a few d and N_1 in Table 1. The estimate (18) is also helpful to choosing parameters under different demand of accuracy, which will be shown in Table 3.

d	13	16	20	26
N_1	5	6	6	6
Bound	4.4×10^{-5}	3.6×10^{-6}	4.5×10^{-7}	4.5×10^{-8}

Table 1: Absolute error bound by (18) under different values of d and N_1 for $n + m \leq 4$.

Moment	Z	Z_{20}/Z	Z_{02}/Z
Maximal error	6.038×10^{-8}	2.030×10^{-8}	1.543×10^{-8}
Moment	Z_{40}/Z	Z_{04}/Z	Z_{22}/Z
Maximal error	4.031×10^{-9}	2.049×10^{-8}	2.098×10^{-8}

Table 2: Maximal absolute error for the 30,000 pairs of (b_1, b_2) .

3.2 Numerical Test

We compare the results calculated by our method and the results calculated by numerical integration to testify the accuracy of our method numerically. The parameters in our method are chosen as $N_1 = 5$, $N_2 = 5$ and $d = 30$. For numerical integration, we use adaptive Simpson's method to control the absolute error less than 10^{-11} . We select randomly 10,000 pairs of b_i for each of the three cases: $b_1, b_2 \leq -d$, $\max(b_1, b_2) > -d$ & $\min(b_1, b_2) \leq -d$, and $b_1, b_2 > -d$, and calculate Z and the moments Z_{nm}/Z where $n + m = 2, 4$. Table 2 shows the maximal absolute errors of Z and Z_{nm}/Z among the 30000 samples, which are under the magnitude of 10^{-8} . In particular, the errors of Z_{nm}/Z are less than 5×10^{-8} . We also examine the distribution of the absolute errors of Z (Figure 1(a)), Z_{20}/Z (Figure 1(b)) and Z_{04}/Z (Figure 1(c)) for the 10000 samples in each of three cases respectively, and find that for most b_i the absolute errors are less than 10^{-10} . Moreover, the numerical test also shows our method is very fast. Calculating all these 30,000 examples, the adaptive Simpson's method with the target accuracy 5×10^{-8} spend 3117.761 seconds while our method only 0.193 seconds. Both routines are written in C and run in the same computer with a CPU clock speed 2.5GHz.

We also give some other suggested values of d , N_1 and N_2 in Table 3 for different demanded accuracy for Z_{nm}/Z , which are also testified numerically with 30,000 random samples. By comparing with the errors in Table 3 and Table 1, we find that the upper bound given by (18) are indicative for the choice of parameters.

Demanded maximal absolute error	5×10^{-5}	5×10^{-6}	5×10^{-7}	5×10^{-8}
d	13	16	20	26
N_1	5	6	6	6
N_2	4	5	6	6

Table 3: Suggested values of parameters d , N_1 and N_2 under different demanded absolute error.

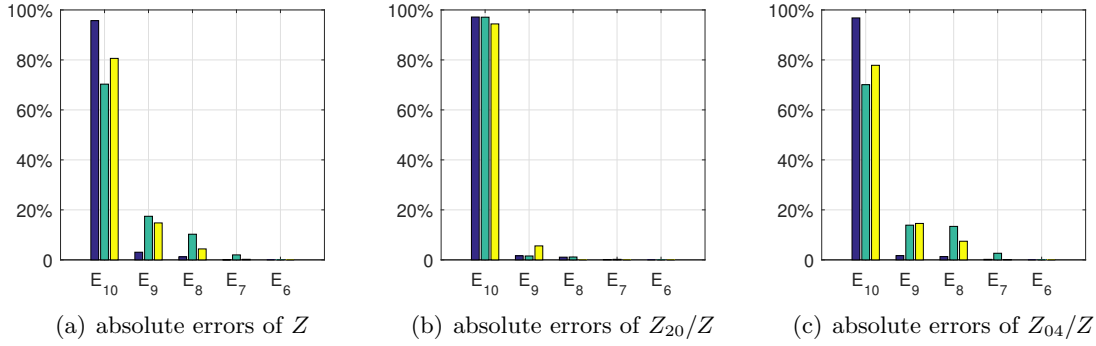


Figure 1: Distribution of error. Blue bars: $b_1, b_2 \leq -d$; Green bars: $\max(b_1, b_2) > -d$ & $\min(b_1, b_2) \leq -d$; Yellow bars: $b_1, b_2 > -d$. E_i represents the interval $[10^{-i-1}, 10^{-i})$ for $i = 7, 8, 9$. $E_{10} = [0, 10^{-10})$ and $E_6 = [10^{-7}, \infty)$.

4 Application to liquid crystals

In this section, we apply our algorithm to a Q -tensor model for rod-like liquid crystals. Compared with the original Landau-de Gennes Q -tensor theory, the model is able to constrain the tensor within the physical range [3], and is closely connected to molecular theory [8]. But the Bingham distribution in the model brings difficulty in numerical simulations. We will explain how our fast algorithm accelerates the computation.

Suppose that the rod-like molecules are confined inside the unit sphere. Then the anchoring effect on the spherical surface will induce defects for the alignment of the molecules. We consider the following simplified free energy,

$$F = \int_{\Omega} dx dy dz \left[(B : (Q + \frac{I}{3}) - \log Z) - \frac{1}{2} \alpha_1 |Q|^2 + \frac{1}{2} \alpha_2 |\nabla Q|^2 \right] + F_p, \quad (23)$$

where the region Ω is chosen as the unit sphere, I is the identity matrix, and

$$Q_{ij}(\mathbf{x}) = \int_{\mathbb{S}^2} (x_i x_j - \frac{1}{3} \delta_{ij}) f(\mathbf{x}|B) dS$$

is a symmetric traceless matrix describing the orientational distribution of rod-like molecules at each spatial point, with $f(\mathbf{x}|B)$ and $Z = Z_{000}(B)$ defined in (1) and (2). Here δ_{ij} is the Kronecker notation. The first two terms in the integral are the bulk energy describing the nematic phase in equilibrium. This bulk energy is the only terms distinct from the phenomenological Landau-de Gennes theory, where the bulk energy is given as a polynomial

$$a_2 \text{tr}(Q^2) - a_3 \text{tr}(Q^3) + a_4 (\text{tr}(Q^2))^2.$$

The gradient term is the energy contribution of the spatial inhomogeneity. The boundary penalty term

$$F_p = \int_{\partial\Omega} dS [Q_{11}xy - Q_{12}(x^2 - \frac{1}{3})]^2 + [Q_{12}z - Q_{13}y]^2 + [Q_{22}xy - Q_{12}(y^2 - \frac{1}{3})]^2 + [Q_{12}z - Q_{23}x]^2$$

is added to enforce the value of Q on the sphere to be approximately

$$Q = \lambda \begin{pmatrix} x^2 - \frac{1}{3} & xy & xz \\ xy & y^2 - \frac{1}{3} & yz \\ xz & yz & z^2 - \frac{1}{3} \end{pmatrix}.$$

In fact, if Q is given as above, then $F_p = 0$. Our aim is to find local minimizers of the energy functional (23) that describe metastable states.

Express B as $B = T \text{diag}(b_1, b_2, 0) T^T$, where T is orthogonal with $\det T = 1$ and can be expressed by Euler angles,

$$T = \begin{pmatrix} \cos \alpha \cos \gamma - \cos \beta \sin \alpha \sin \gamma & \cos \gamma \sin \alpha + \cos \alpha \cos \beta \sin \gamma & \sin \beta \sin \gamma \\ -\cos \beta \cos \gamma \sin \alpha - \cos \alpha \sin \gamma & \cos \alpha \cos \beta \cos \gamma - \sin \alpha \sin \gamma & \cos \gamma \sin \beta \\ \sin \alpha \sin \beta & -\cos \alpha \sin \beta & \cos \beta \end{pmatrix}.$$

In this case, $Q = T \text{diag}(q_1, q_2, q_3) T^T$, where the eigenvalues are given by $q_1 = Z_{20}(b_1, b_2)/Z_{00}(b_1, b_2)$, $q_2 = Z_{02}(b_1, b_2)/Z_{00}(b_1, b_2)$, and $q_3 = 1 - q_1 - q_2$.

We use the spherical coordinates (r, θ, ϕ) to represent the position, i.e.,

$$x = r \sin \theta \cos \phi, \quad y = r \sin \theta \sin \phi, \quad z = r \cos \theta. \quad (24)$$

The integral becomes $\int(\cdot) dx dy dz = \int(\cdot) r^2 \sin \theta dr d\theta d\phi$, and the gradient term becomes

$$|\nabla Q|^2 = |\partial_r Q|^2 + \frac{1}{r^2} |\partial_\theta Q|^2 + \frac{1}{r^2 \sin^2 \theta} |\partial_\phi Q|^2. \quad (25)$$

The free energy is discretized at $N \times N \times N = 32^3$ Gaussian quadrature nodes (r_j, θ_k, ϕ_l) in $[0, 1] \times [0, \pi] \times [0, 2\pi]$. At each node $(b_1, b_2, \alpha, \beta, \gamma)^{jkl}$ act as the basic variables, from which Q^{jkl} is computed. The gradient term is computed using the spectral-collocation method. From the value of Q at the discretized nodes, a polynomial

$$Q(r, \theta, \phi) = \sum_{j=0}^{N-1} \sum_{k=0}^{M-1} \sum_{l=0}^{L-1} c_Q^{jkl} r^j \theta^k \phi^l$$

is constructed through interpolation. The derivatives about (r, θ, ϕ) , as well as the values on the boundary, are then computed from the above polynomial. We refer to [19] where the details about the spectral-collocation method are illustrated. The free energy is minimized using the BFGS method (see, for instance, [2]). In the iteration we need to compute the derivatives of F about $(b_i)^{jkl}$, where fourth moments are involved. For instance,

$$\frac{\partial}{\partial b_1} Q = T \text{diag} \left(\frac{\partial q_1}{\partial b_1}, \frac{\partial q_2}{\partial b_1}, \frac{\partial(-q_1 - q_2)}{\partial b_1} \right) T^T,$$

where

$$\frac{\partial q_1}{\partial b_1} = \frac{Z_{40} Z_{00} - Z_{20}^2}{Z_{00}^2}.$$

It is worth pointing out that at each point, the value of Q and Z are computed from B . Therefore, our algorithm is executed $O(N^3)$ times in each BFGS iteration step, which greatly accelerates the simulation. Another thing is that the Bingham distribution remains the same

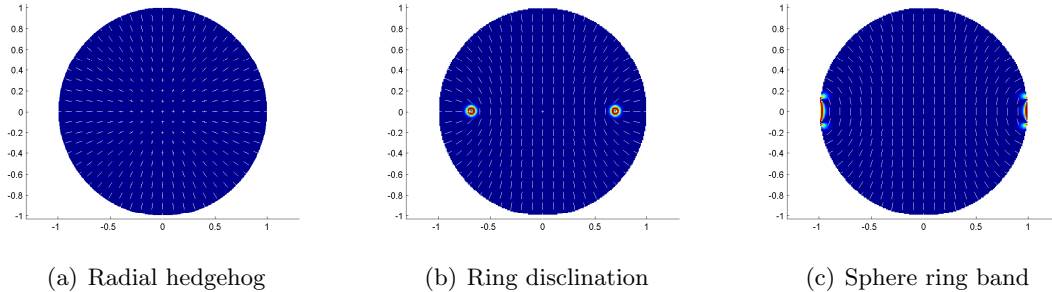


Figure 2: Three axisymmetric defect patterns, shown by the slice of x_2 - x_3 plane, where x_3 is the axis of symmetry. White rods represent principal eigenvectors. The background color describes the biaxiality μ , with red indicates biaxial and blue indicates uniaxial. In all three cases $\alpha_2 = 0.04$, and α_1 are chosen as: (a) $\alpha_1 = 11$; (b) $\alpha_1 = 16$; (c) $\alpha_1 = 22$.

when we alter the parameters $\alpha_{1,2}$, the domain (from sphere to cylinder or ellipse, etc.), and add some terms like in [8]. Thus our algorithm is suitable for all these cases.

Before looking at the results, we first define the biaxiality. When $Q \neq 0$, we say Q is uniaxial if it has two identical eigenvalues, and is biaxial if it has distinct eigenvalues. Note that $\text{tr}Q = 0$. The biaxiality is measured by

$$\mu = 1 - 6 \frac{(\text{tr}Q^3)^2}{(\text{tr}Q^2)^3}.$$

For uniaxial Q , we have $\mu = 0$; for biaxial Q , we have $0 < \mu \leq 1$. We examine the defect pattern under different α_1 and α_2 . At each point, the favored direction of the rod-like molecules is the principal unit eigenvector \mathbf{n} of Q . While Q is continuous in the unit sphere, \mathbf{n} might be discontinuous at the points where $Q = 0$ or Q has two identical positive eigenvalues. Defect patterns are classified by the configuration of these points.

We fix $\alpha_2 = 0.04$ and let α_1 vary. Three defect patterns are observed and drawn in Figure 2: radial hedgehog (Figure 2(a)), when $\alpha_1 = 11$; ring disclination (Figure 2(b)), when $\alpha_1 = 16$; sphere ring band (Figure 2(c)), when $\alpha_1 = 22$. In the radial hedgehog pattern, Q is uniaxial everywhere with the principal eigenvector along the radial direction. The sphere center, where $Q = 0$, is the only point defect. In the ring disclination pattern, the points where Q has two identical positive eigenvalues form a circle in the x - y plane, round which is a torus of biaxial region. In the sphere ring band pattern, the points where $Q = 0$ form two rings on the spherical surface. In the band between these two rings on the spherical surface, Q has two identical positive eigenvalues. A strong biaxial region is observed inside the sphere near the band. The last pattern is not found in the Landau-de Gennes theory [9]. We believe that this novel pattern come from the term $B : (Q + I/3) - \log Z$, since it is the only term different from the Landau-de Gennes theory. Hence, it is necessary for this model to be further examined.

5 Conclusion

We develop a fast and accurate algorithm to evaluate the moments of Bingham distribution. Numerical test shows that it is remarkably faster than direct numerical quadrature, while

maintaining high accuracy. We apply the algorithm to the liquid crystal model that contains the Bingham distribution, which is able to constrain the order parameters within the physical range. We examine the defect patterns of liquid crystals confined inside a sphere and find a novel pattern, suggesting that the model be examined thoroughly and compared with the Landau-de Gennes theory in future studies. Armed with our algorithm, these studies will become much less expensive computationally.

Acknowledgment Pingwen Zhang is supported by National Natural Science Foundations of China (Grant No. 11421101 and No. 1142110001).

References

- [1] V Alastrué, P Sáez, MA Martínez, and M Doblaré. On the use of the Bingham statistical distribution in microsphere-based constitutive models for arterial tissue. *Mechanics Research Communications*, 37(8):700–706, 2010.
- [2] Mordecai Avriel. *Nonlinear programming: analysis and methods*. Courier Corporation, 2003.
- [3] John M Ball and Apala Majumdar. Nematic liquid crystals: from Maier-Saupe to a continuum theory. *Molecular crystals and liquid crystals*, 525(1):1–11, 2010.
- [4] Christopher Bingham. An antipodally symmetric distribution on the sphere. *The Annals of Statistics*, pages 1201–1225, 1974.
- [5] Maxime Descoteaux, Rachid Deriche, Thomas R Knösche, and Alfred Anwander. Deterministic and probabilistic tractography based on complex fibre orientation distributions. *Medical Imaging, IEEE Transactions on*, 28(2):269–286, 2009.
- [6] J Feng, CV Chaubal, and LG Leal. Closure approximations for the Doi theory: Which to use in simulating complex flows of liquid-crystalline polymers? *Journal of Rheology (1978-present)*, 42(5):1095–1119, 1998.
- [7] Massimiliano Grosso, Pier L Maffettone, and Francois Dupret. A closure approximation for nematic liquid crystals based on the canonical distribution subspace theory. *Rheologica acta*, 39(3):301–310, 2000.
- [8] Jiequn Han, Yi Luo, Wei Wang, Pingwen Zhang, and Zhifei Zhang. From microscopic theory to macroscopic theory: a systematic study on modeling for liquid crystals. *Archive for Rational Mechanics and Analysis*, 215(3):741–809, 2014.
- [9] Yucheng Hu, Yang Qu, and Pingwen Zhang. On the disclination lines of nematic liquid crystals. *Communications in Computational Physics*, 19:354–379, 2016.
- [10] John T Kent. Asymptotic expansions for the Bingham distribution. *Applied statistics*, pages 139–144, 1987.
- [11] JT Kent, JC Briden, and KV Mardia. Linear and planar structure in ordered multivariate data as applied to progressive demagnetization of palaeomagnetic remanence. *Geophysical Journal International*, 75(3):593–621, 1983.

- [12] JL Kirschvink. The least-squares line and plane and the analysis of palaeomagnetic data. *Geophysical Journal International*, 62(3):699–718, 1980.
- [13] Alfred Kume, SP Preston, and Andrew TA Wood. Saddlepoint approximations for the normalizing constant of Fisher–Bingham distributions on products of spheres and Stiefel manifolds. *Biometrika*, 100(4):971–984, 2013.
- [14] Alfred Kume and Andrew TA Wood. Saddlepoint approximations for the Bingham and Fisher–Bingham normalising constants. *Biometrika*, 92(2):465–476, 2005.
- [15] Karsten Kunze and Helmut Schaeben. The bingham distribution of quaternions and its spherical radon transform in texture analysis. *Mathematical Geology*, 36(8):917–943, 2004.
- [16] Yixiang Luo and Jie Xu. <https://github.com/yixiangLuo/Bingham-moment-function/>, 2016.
- [17] Thomas P Minka. Automatic choice of dimensionality for PCA. In *NIPS*, volume 13, pages 598–604, 2000.
- [18] Tullis C Onstott. Application of the Bingham distribution function in paleomagnetic studies. *Journal of Geophysical Research: Solid Earth*, 85(B3):1500–1510, 1980.
- [19] Jie Shen, Tao Tang, and Li-Lian Wang. *Spectral methods: algorithms, analysis and applications*, volume 41. Springer Science & Business Media, 2011.
- [20] Han Wang, Kun Li, and Pingwen Zhang. Crucial properties of the moment closure model FENE-QE. *Journal of Non-Newtonian Fluid Mechanics*, 150(2):80–92, 2008.
- [21] Feng Zhao, Jian Peng, and Jinbo Xu. Fragment-free approach to protein folding using conditional neural fields. *Bioinformatics*, 26(12):i310–i317, 2010.